Journal of Constructional Steel Research 122 (2016) 14–24

Contents lists available at ScienceDirect

Journal of Constructional Steel Research

Investigations on the mechanical behavior of suspend-dome with semirigid joints

Zhihua Chen [a,b,*], Hao Xu [b], Zhongwei Zhao [b], Xiangyu Yan [c], Bingzhen Zhao [b]

[a] State Key Laboratory of Hydraulic Engineering Simulation and Safety, Tianjin University, Tianjin 300072, China
[b] Department of Civil Engineering, Tianjin University, Tianjin 300072, China
[c] Tianjin University Research Institute of Architectural Design and Urban Planning, Tianjin University, Tianjin 300072, China

ARTICLE INFO

Article history:
Received 22 September 2015
Received in revised form 21 January 2016
Accepted 28 January 2016
Available online 3 February 2016

Keywords:
Bending stiffness
Double element method
Geometric imperfection
Joint stiffness
Suspend-dome structures

ABSTRACT

Most finite element models of actual projects developed using general finite element software are rigid or hinge connected. These models are inconsistent with the actual situations of most actual projects that are semirigid jointed. The double element method was adopted to estimate the influence of joint stiffness on the mechanical behavior of suspend-dome structures. First, the accuracy of this method was validated. This approach was adopted to analyze the influence of joint stiffness on the mechanical behavior of the overall structure. Buckling, modal, and dynamic response analyses were conducted. The effect of joint stiffness on the buckling capacity of suspend-dome and single-layer latticed shell was derived and compared. The influence of joint stiffness on the characteristics of natural vibration was also determined. Finally, seismic response analysis was conducted to estimate the influence of joint stiffness on structural dynamic response. Results indicate that rigid connected finite element models may be unreliable to calculate dynamic response during the design phase.

© 2016 Elsevier Ltd. All rights reserved.

1. Introduction

Suspend-dome is a new style of space-reticulated structure, which is formed by combining a single-layer reticulated shell and cable–strut system. Compared with traditional single-layer reticulated shell structures, suspend-domes exhibit a more uniform spatial stiffness distribution, has less thrust on supports, and shows a stronger spanning capacity [1].

Researchers examined the performance of the suspend-dome structure from the experimental and numerical viewpoints [2,3,4,5,6]. Current research demonstrate that the buckling capacity of the pin-connected suspend-dome is lower compared with that of the rigidly connected suspend-dome [7]. However, the influence of joint stiffness has not been quantitatively verified.

The upper latticed shells usually consist of thousands of components that are connected by joints. The stiffness of connections was determined to be one of the factors that significantly affect the behavior of space structures, and these effects were investigated numerically and experimentally [8,9]. In the actual design process, the joints are assumed to be either pinned or rigid joints. This assumption may result in a significant deviation from the actual condition. Lattice shells with semirigid joints can provide a good solution for space structures. Thus, including joint stiffness in the numerical model is necessary.

Predicting the mechanical behavior of joints is the first step in analyzing spatial structures with semirigid joints. Many studies were conducted to analyze the mechanical behavior of joints in space structures [10]. López et al. [11,12], Ma et al. [13], Fan et al. [14], and Kato et al. [15] verified that the rigidity of joints is an important factor that influences the behavior of a single-layer latticed dome. Fan [8,16,17,18] systematically conducted experimental and numerical analyses to investigate the influence of joint stiffness on the mechanical behavior of latticed shells. Finite element method and experimentation were the main approaches to examine semirigid joints [19].

However, the studies mainly discuss the joints itself or simple structures, such as steel frames [20,21,22,23,24,25]. The axial direction, length, and cross section of the spatial latticed structures, which consist of thousands of components, significantly vary. Establishing numerical models that consider the influence of joint stiffness is time-consuming and tedious. A few of these numerical reticulated shell models were used because they are complex and relevant studies are limited. A convenient and efficient method that integrates joint stiffness in numerical models of spatial latticed structures has not yet been developed. In this study, double element method was adopted to investigate the influence of joint stiffness on the mechanical behavior of the suspend-dome.

2. Double element method

Research on the stiffness of joints and their effects on the behavior of structures has been an area of interest to engineers and scientists in recent years, and many applicable conclusions have been achieved.

* Corresponding author at: State Key Laboratory of Hydraulic Engineering Simulation and Safety, Tianjin University, Tianjin 300072, China.
E-mail address: zhchen@tju.edu.cn (Z. Chen).

http://dx.doi.org/10.1016/j.jcsr.2016.01.021
0143-974X/© 2016 Elsevier Ltd. All rights reserved.

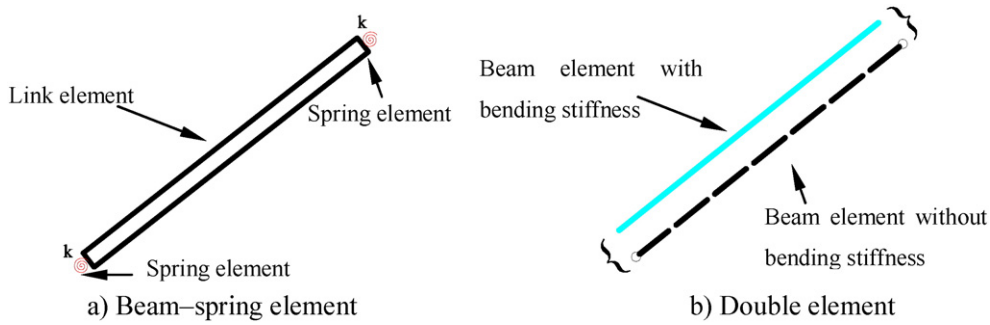

Fig. 1. Numerical model considering joint stiffness.

However, no applicable method that considers joint stiffness in a general finite element software has been developed. A simplified method integrating joint stiffness was proposed in this study.

This method assumes that every component of a latticed shell is composed of two elements, namely, beam element with only bending stiffness and beam element without bending stiffness.

The rotation angle of the beam under action of moment M, as shown in Fig. 2, can be calculated using Eq. (1) for a beam with a constant cross section. The bending stiffness of the beam can be represented by Eq. (2).

The significant influence of the stiffness of joints on the mechanical performance of lattice shells has been validated [16], particularly for buckling behavior. In a numerical model, the joints of latticed shells were assumed to be a rigid or simple joint. In fact, almost all joints in structures exhibit some degree of semirigid behavior. For these kinds of structures, the stiffness of action of joints can be substituted by spring element [18], as indicated in Fig. 1(a). The rotation angle of this system under the action of moment M can be calculated through Eq. (3). The bending stiffness of the beam can be represented by Eq. (4), through which it can be concluded that, when the joint stiffness k was equivalent to Eq. (2), it is sufficiently large.

López [21] proposed the use of an elasto-plastic cylinder located between the tube and the balls to simulate the bolt, which is time-consuming and work-intensive to establish the numerical models of latticed shells because of the large amount of components. This study proposed the double element method to consider joint stiffness, as shown in Fig. 1(b). That is, each component of latticed shells is composed of two elements, namely, beam element with bending stiffness of the component and beam element without bending stiffness.

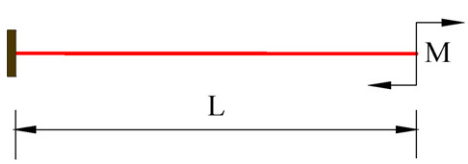

Fig. 2. Beam under the action of moment.

$$\theta = \int_l \frac{M}{EI}\mathrm{d}l = \frac{Ml}{EI}, \tag{1}$$

$$\frac{M}{\theta} = \frac{EI}{l}, \tag{2}$$

$$\theta = \int_l \frac{M}{EI}\mathrm{d}l + 2 \times \frac{M}{K} = M\left(\frac{l}{EI} + \frac{2}{K}\right), \tag{3}$$

$$\frac{M}{\theta} = \frac{1}{\frac{l}{EI} + \frac{2}{K}} = \frac{EI}{l} \times \frac{K}{K + \frac{2EI}{l}}, \tag{4}$$

where θ is the rotation angle of the beam, I is the moment of inertia of the members, $E = 206$ GPa represents Young's modulus, and K is the bending stiffness of the spring element.

We assume that α indicates the overall bending stiffness factor of the beam element and β indicates the bending stiffness factor that only considers the joint bending stiffness, as shown in Eqs. (5) and (6). Eq. (7) denotes the relationship between α and β. Fig. 3 indicates the curves between α and β. The overall bending stiffness factor tends to 1 with the increase in β.

$$\alpha = \frac{K}{K + \frac{2EI}{l}}, \tag{5}$$

$$\beta = \frac{K}{\frac{EI}{l}}, \tag{6}$$

$$\alpha = \frac{\beta}{\beta + 2}. \tag{7}$$

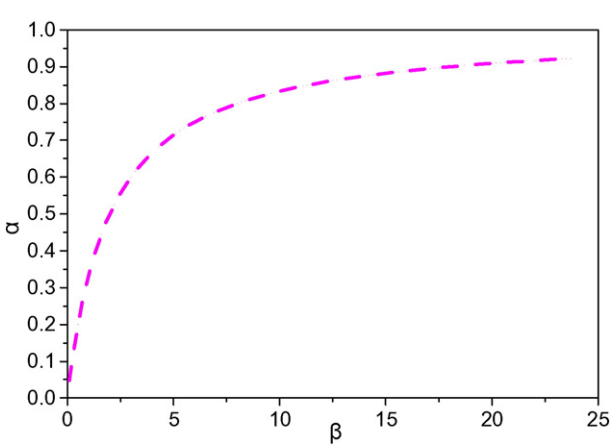

Fig. 3. Curves between α and β.

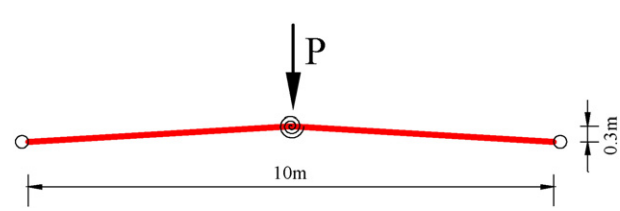

Fig. 4. Two-member structure with semirigid joint.

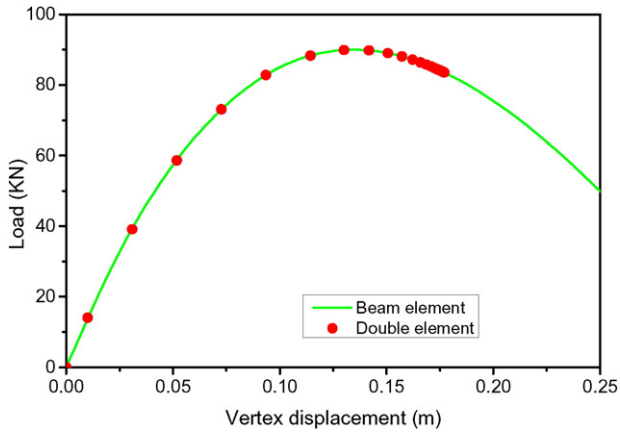

Fig. 5. Comparison of the results derived by beam element and double element.

The general finite element software ANSYS was adopted to obtain the load versus displacement curves of structures. The two-member structure was first established by ordinary beam element (BEAM4) in ANSYS [26].

Only the bending stiffness was assigned a real constant for a beam element with bending stiffness in the double element. For the beam element without bending stiffness in the double element, the BEAM4 element in ANSYS was also employed. However, the value of bending stiffness was low. Thus, the beam element can be assumed to be a link element.

The two elements share the same nodes at both ends. Thus, the displacement vector of the two elements is equal to each other. This step ensures that the two elements coordinate with each other. Thus, the two elements can be assumed as one element with special functions. Thus, Eq. (8) is equal to Eq. (9) plus Eq. (10). The beam element in the double element only includes bending stiffness and can be adjusted easily to consider the influence of joint stiffness.

A two-member structure was adopted to validate the effectiveness of the proposed double element method, (See Fig. 4.). The cross-section area $A = 0.0048\ \mathrm{m}^2$ and moment of inertia $I = 6.28 \times 10^{-6}\ \mathrm{m}^4$ were inputted as real constants. The structure was established by the double element method. This structure is the link element with area $A = 0.0048\ \mathrm{m}^2$ and beam element with $I = 6.28 \times 10^{-6}\ \mathrm{m}^4$. The area of the beam was set at a small value. Thus, its axial strength can be ignored.

Fig. 5 shows the results derived by beam element and double element. The results derived by double element are consistent with that obtained by beam element. Fig. 6 shows the load versus displacement curves with different bending stiffness factors. These results indicate that joint stiffness significantly affects the critical load of the two-member structure. The results also demonstrate that joint stiffness can be considered by adjusting beam bending stiffness factor α.

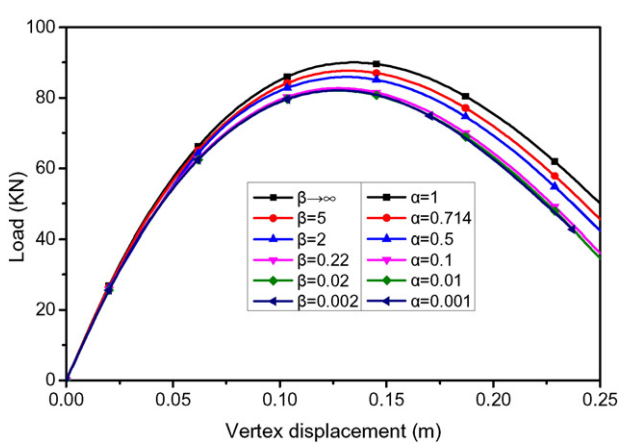

Fig. 6. Load versus displacement curves with different bending stiffness factors.

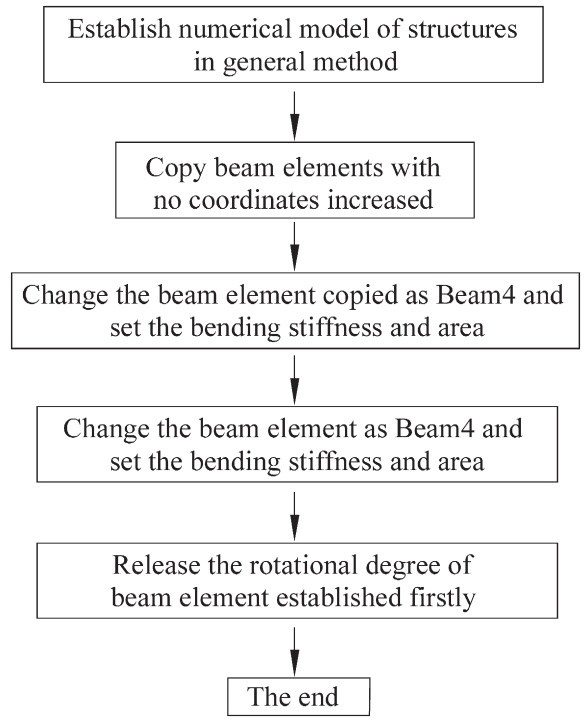

Fig. 7. Flowchart of the simplified double element method.

3. Finite element model

A suspend-dome structure was designed to analyze the influence of joint stiffness on the mechanical behavior of suspend-dome structures. The roof of the building is spherical with a diameter of 108 m and a vector height of 25.5 m, as shown in Fig. 8(a). For the suspend-dome, the Lamella–Kiewit composite single-layer lattice shell with a span of 108 m was adopted. Seven rings of cable–strut systems were arranged under the single-layer lattice shell with steel pipes of φ203 mm × 6 mm, φ219 mm × 7 mm, φ245 mm × 7 mm, φ273 mm × 8 mm, and φ299 mm × 8 mm as the principal members of the single-layer shell. In the lower suspend-dome, steel pipes of φ219 mm × 7 mm were used as vertical struts. Steel bars with a diameter of 80 mm were utilized as the radial bars. Steel cables of φ7 mm × 121 mm functioned as four outer hoop cables. Steel cables of φ7 mm × 73 mm were used as the three inner hoop cables. The pre-stresses in the hoop cables were uniformly set to 127, 420, 390, 530, 810, 1242, and 2060 kN. The steel pipes measuring φ1000 mm × 16 mm and φ1500 mm × 24 mm were used as the principal members of the upper arches, whereas steel pipes of φ325 mm × 8 mm, φ377 mm × 10 mm, and φ426 mm × 10 mm were used as the principal members of the strut between the suspend-dome and the arches. The elastic moduli of the steel (Q345) and the cable were 2.06×10^5 and $1.8 \times 10^5\ \mathrm{N/mm}^2$, respectively. The boundary conditions were assumed as simply supported. Two rings of bearings were set in this structure, as shown in Fig. 8(b): one is located at the outmost ring and the other is located at the fourth outmost ring. The bearing is free in the radial direction, the vertical direction is fixed, and the hoop direction is elastically restrained with a stiffness coefficient of 2.8×10^5 kN/m.

The finite element model of the analyzed structures was established in the general finite element software ANSYS. The hoop cables, steel bars, and bearings were modeled by Link10, Link8, and Combin39, respectively. Each component of the upper latticed shell was simulated

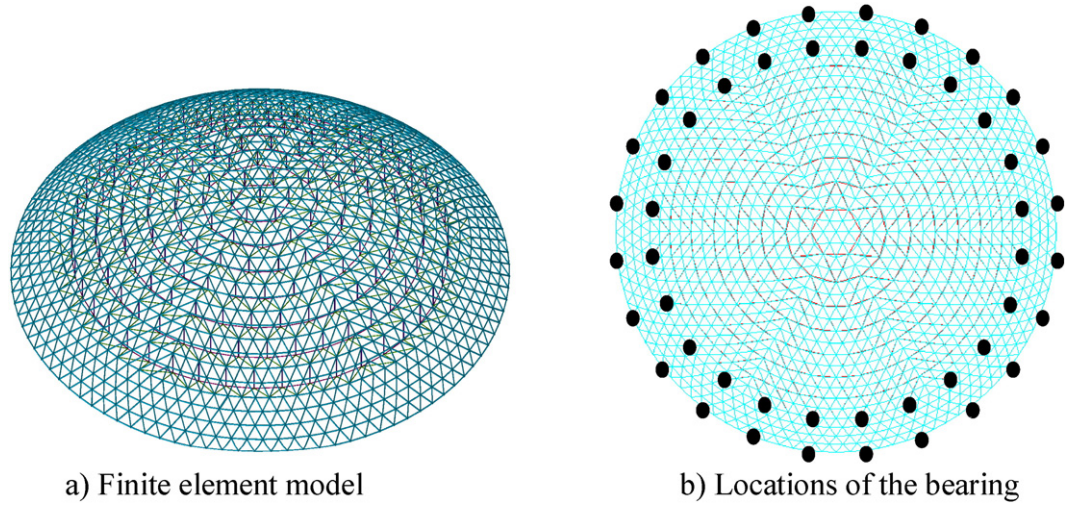

Fig. 8. Schematic diagram of the suspend-dome structure.

by BEAM188 and BEAM4. The BEAM188 element was pin jointed by releasing the "Endrelease" command.

The upper latticed shell structure was established by BEAM188 element, and the cross sections were assigned according to the actual situation. The beam element was copied without changing the coordinate, and the element type was changed to BEAM4 to function the role of a beam element with no axial strength, as indicated in Fig. 1(b). Only the bending stiffness of BEAM4 was assigned a real constant. The rotational degrees about the *x*- and *y*-directions of BEAM188 were released by the "Endrelease" command. The flowchart of the double element is shown in Fig. 7. Establishing the numerical model is efficient. The finite element model of the suspend-dome structure is presented in Fig. 8.

4. Static analyses: linear and nonlinear buckling

In this section, the effects of connection rigidity on the buckling capacity of the suspend-dome system were investigated. First, eigenvalue buckling analysis was conducted. Then, nonlinear buckling analysis was conducted for the suspend-dome and the single-layer latticed shell. Finally, the results were compared. The single-layer latticed shell indicates the upper latticed shell of the suspend-dome.

4.1. Linear buckling analysis

The Eigenvalue buckling analysis predicts the theoretical buckling capacity (the bifurcation load) of an ideal linear elastic structure. However, imperfections and nonlinearities prevent most real-world structures from achieving the theoretical elastic buckling capacity. Nevertheless, the Eigenvalue buckling analysis provides an upper bound for the critical load, along with the buckling mode, which provides engineers valuable information about the buckling behavior of the system. The results of the Eigenvalue buckling analysis of the suspend-dome and the corresponding single-layer dome under different conditions are analyzed.

Buckling analysis only considered the dead load, including weight of the components and roof dead load, which is 0.14 kN/m^2.

Fig. 9 shows the buckling mode when the components were rigidly connected. The figure clearly indicates that buckling occurs at the central part of the structure. The upper latticed shell was divided into different parts, as shown in Fig. 10, to investigate the influence of the stiffness of joints located in different parts of the structure. The joint stiffness

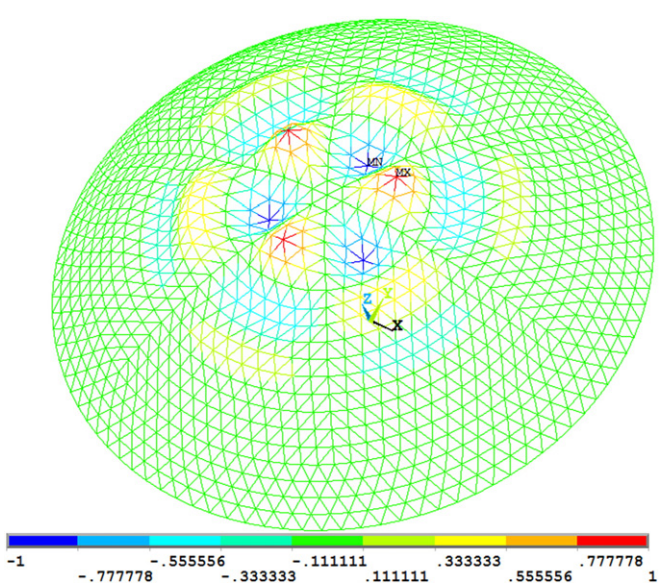

Fig. 9. Buckling mode of rigid joint structures.

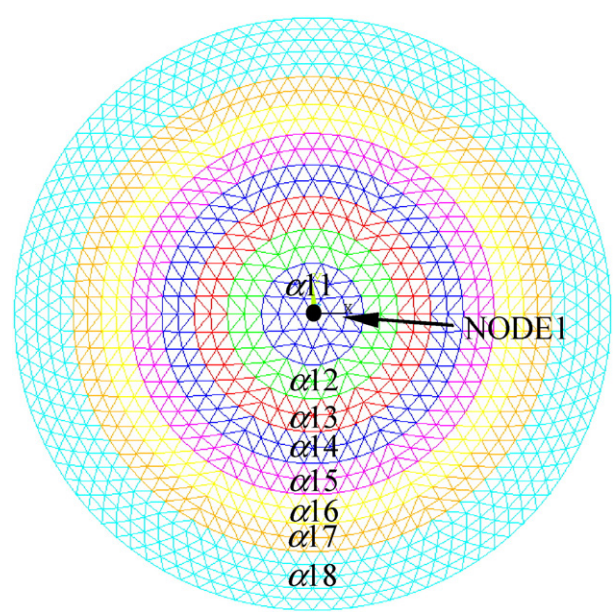

Fig. 10. Stiffness factor of each part of the overall structure.

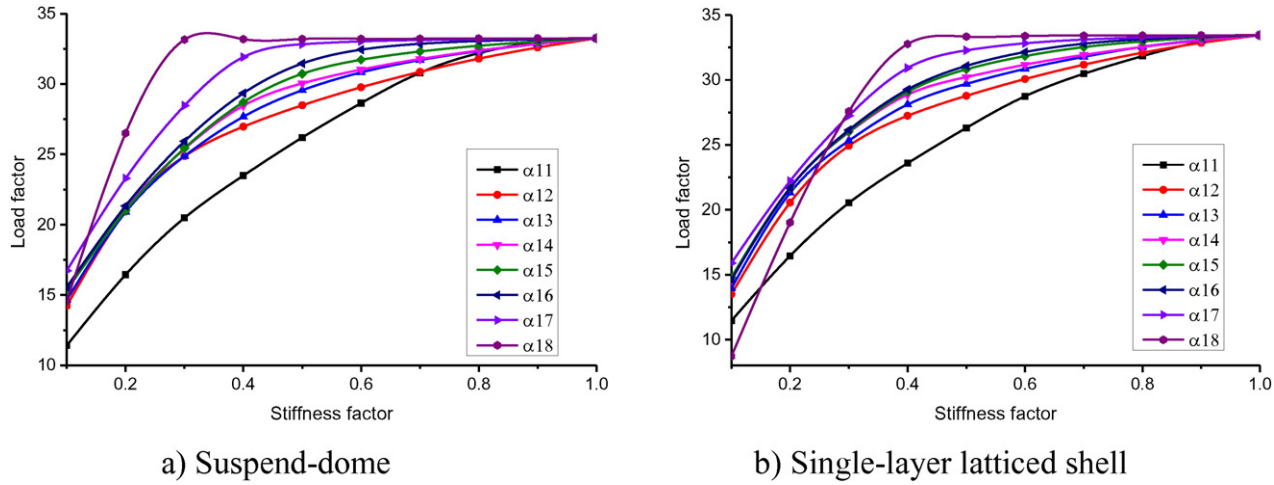

Fig. 11. Curves of buckling load to stiffness factor.

factor of each part was adjusted separately from 0.1 to 1 in steps of 0.1, which indicate pin jointed and rigid joint structures. Buckling critical load factor was extracted and compared, as shown in Fig. 11.

The results shown in Fig. 11 indicate that the changing tendency of the buckling capacity of the suspend-dome to the stiffness factor is almost the same as that of the upper single-layer latticed shell. The Eigenvalue buckling analysis can only consider the initial structural stiffness. Thus, the influence of the cable–strut system cannot be fully integrated. Joint stiffness located in different parts of the structure variably affect buckling capacity. When the joint stiffness of one part was adjusted, the other different parts remain rigidly connected. The joint stiffness factors were changed from 0.1 to 1, which can be assumed to be pin jointed and rigid joint. The upper components of the structure influence buckling capacity more than the lower components. Buckling often occurs at the upper part of the structure. $\alpha 18$ influenced buckling capacity when it decreased to 0.3 and 0.4 for the suspend-dome structure and single-layer latticed shell. $\alpha 11$ immediately influenced buckling capacity when it was changed.

The upper latticed shell was divided into hoop components and the other components, as shown in Fig. 12, to investigate the influence of the joint stiffness of the hoop components on structural buckling capacity. Fig. 12(a) shows the symbol of the stiffness factor of each of the circle hoop components.

Fig. 13 shows the changing tendency of the buckling capacity, along with the stiffness factor of each circle hoop component. The results indicate that all of the joint stiffness values of the hoop components has almost no influence on buckling capacity. The effect of hoop components located at the upper part of the structure is greater than that of the lower hoop components. The joint stiffness of the hoop components of the lower 11 circles does not affect structural buckling capacity.

Fig. 14 shows the influence of all hoop components and the other components on buckling capacity. When the joint stiffness factor of the hoop components changes from 1 to 0.1, the load factor changes from 33.2 to 24.9. The reduction factor is 75%. The load factor changes from 33.2 to 11.3 for the other components, and the reduction factor is 34%. These results indicate that the influence of the hoop components is lesser than that of the other components.

4.2. Nonlinear buckling analysis

The Eigenvalue buckling analysis predicts the theoretical buckling capacity (the bifurcation load) of an ideal linear elastic structure, which is almost nonexistent in an actual project. Nonlinear buckling analysis was conducted to investigate buckling behavior more thoroughly. The arc-length method [27,28] is employed to obtain the total load–displacement equilibrium path.

The arc-length method is adopted during the entire numerical simulation. The arc-length method is suitable for nonlinear static equilibrium solutions of unstable problems. Applications of the arc-length method involve the tracing of a complex path in the load–displacement response into the buckling/post-buckling regimes.

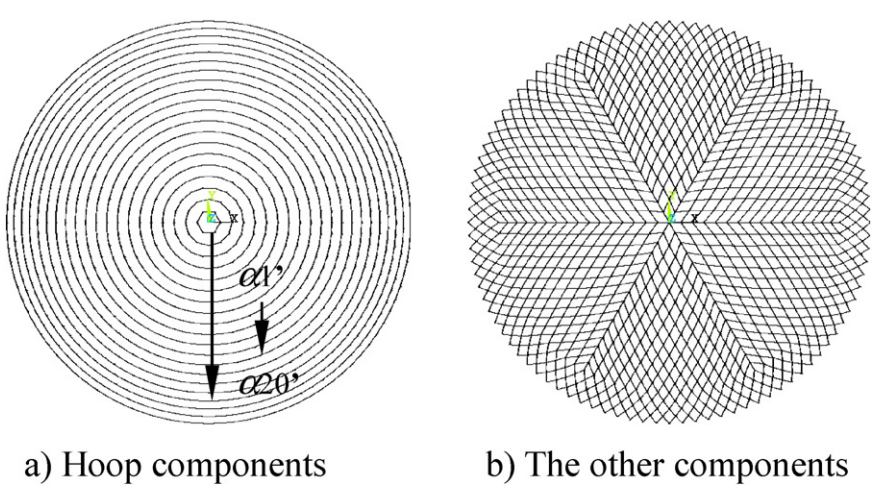

Fig. 12. Components of the upper latticed shell.

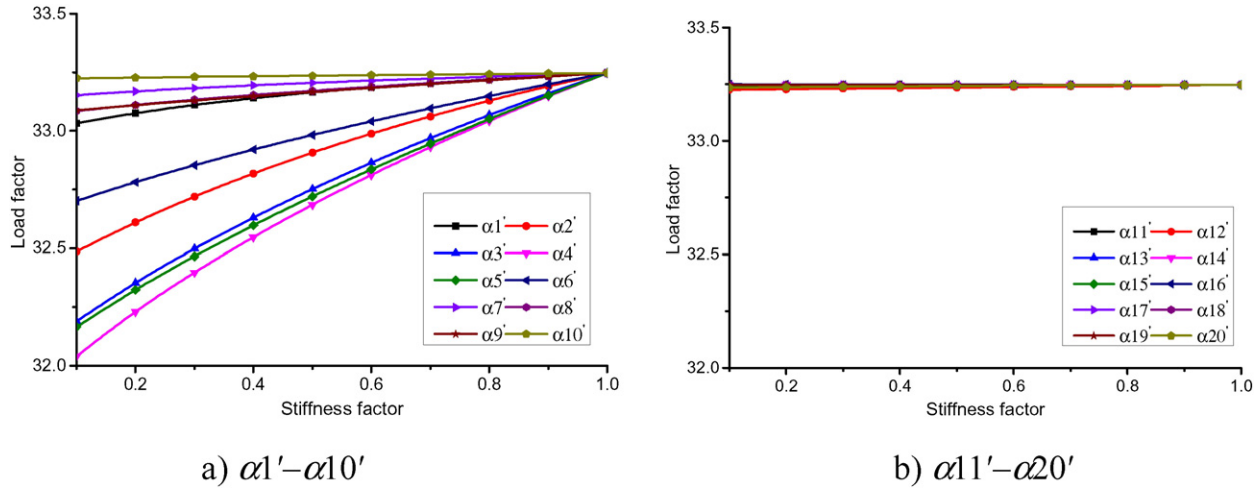

Fig. 13. Influence of the stiffness factor of the hoop components.

The arc-length method was activated by the "ARCLEN" command in ANSYS finite element code, and the minimum and maximum multipliers for the arc-length radius were set. The reference arc-length radius is calculated from the load or displacement increment of the first iteration of the first substep, as follows:

$$\text{Reference Arc}-\text{Length Radius} = \text{Total Load (or Displacement)}/\text{NSBSTP}, \tag{8}$$

where NSBSTP is the number of substeps specified on the NSUBST command. The factors MAXARC and MINARC are employed to define the limits of the arc-length radius by adopting the following formulas:

$$\text{Lower Limit} = \text{MINARC} \times (\text{Reference Arc}-\text{Length Radius}), \tag{9}$$

$$\text{Upper Limit} = \text{MAXARC} \times (\text{Reference Arc}-\text{Length Radius}). \tag{10}$$

A new arc-length radius is first calculated based on the arc-length radius of the previous substep and the solution behavior. Then, the newly calculated arc-length radius is further modified so that it falls between the range of the upper and lower limits. If the solution does not converge even when the lower limit of the arc-length radius is used, then the solution will be terminated.

In this study, geometric nonlinearity was considered by the "NLGEOM,ON" command. The arc-length radius should not be excessively large or small to avoid the "drift back" problem. In this study, the number of substeps was set to 500. The MAXARC and MINARC were set to 5 and 0.001, respectively.

Dome structures are sensitive to geometric imperfection, which is unavoidable during fabrication. In the fundamental mode imperfection method, the imperfection distribution is assumed to be consistent with the first buckling mode. Generally, the buckling capacity that is calculated by the fundamental mode imperfection method is the lowest among all the other modes and is, therefore, the most critical. In this study, nonlinear elastic analysis is conducted to derive the buckling capacities of the domes with $L/300$ [29] maximum nodal imperfections, where L indicates the span of the domes.

Fig. 15 shows the curves of vertical load factor and displacement at node 1 when stiffness factor α was given a different value. The results indicate that the buckling capacity of the suspend-dome is significantly higher than that of the single-layer latticed shell whatever the value of the stiffness factor. The high efficiency of suspend-dome structures was reflected. The buckling capacity of the suspend-dome and single-layer latticed shell is positively correlated with the joint stiffness factor. Geometrical imperfection will reduce buckling capacity whatever the value of the stiffness factor for suspend-dome structures. Joint stiffness significantly affects the buckling capacity of suspend-dome structures. The rigidly jointed model will overestimate structural buckling capacity. Thus, joint stiffness should be considered in calculating the structural buckling capacity for suspend-dome structures.

Meanwhile, the results shown in Fig. 15(a), (b) and (c) reveal that the structures with imperfections seem to be more rigid than the elements without imperfections. This outcome is caused by the location of node 1 and the structural deformation under load before buckling occurs. Geometric imperfection was applied according to the buckling mode shown in Fig. 9. Thus, nonlinear buckling analysis was first conducted. The displacement of node 1 was calculated based on the deformed structure. Thus, the structures with imperfections may seem more rigid.

Fig. 16(a) shows the changing tendency of the critical load factor of the suspend-dome along with the stiffness factor. Geometrical imperfection reduces the critical load factor in almost the same degree when stiffness factor α is greater than 0.3. The changing tendency indicates that the critical load factor is sensitive to geometrical imperfection when stiffness factor α is less than 0.3. This condition shows that the pin jointed structures are almost nonexistent in an actual project. Thus, joint stiffness has no effect on geometrical imperfection. The influence factor of geometrical imperfection on the buckling capacity of the suspend-dome in this study can be set to 0.7.

Fig. 16(b) shows the changing tendency of buckling capacity along with the stiffness factor. The results demonstrate that geometrical imperfection has almost no influence on the buckling capacity of the single-layer latticed shell when the joint stiffness of the structure is

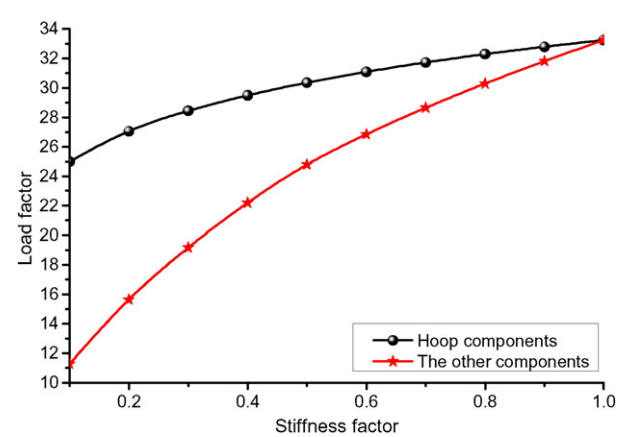

Fig. 14. Influence of the hoop components and the other components.

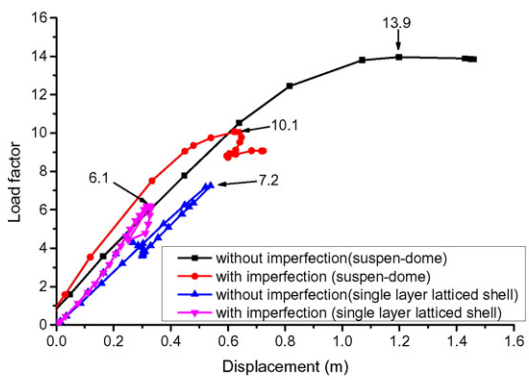

a) Curves of load factor–displacement when $\alpha = 1$

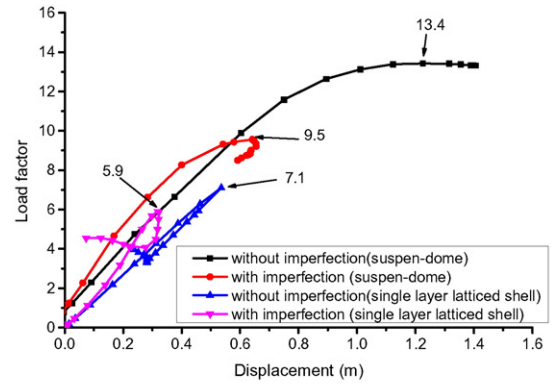

b) Curves of load factor–displacement when $\alpha = 0.9$

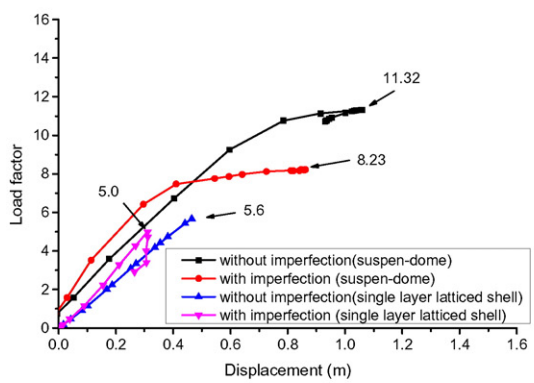

c) Curves of load factor–displacement when $\alpha = 0.6$

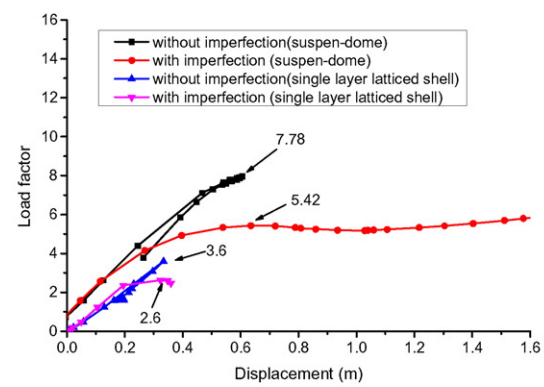

d) Curves of load factor–displacement when $\alpha = 0.3$

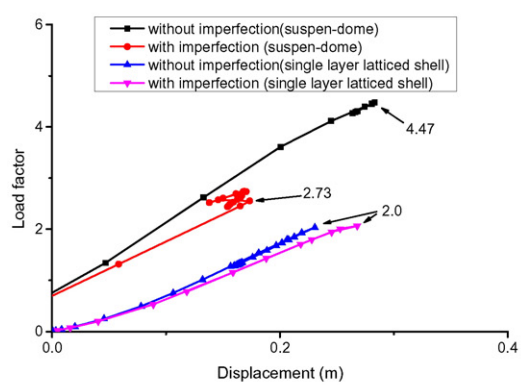

e) Curves of load factor–displacement when $\alpha = 0.1$

Fig. 15. Curves of vertical load factor and displacement at node 1.

sufficiently small. The influence factor of the geometrical imperfection on the buckling capacity of the single-layer latticed shell can be set to 0.8.

5. Dynamic analyses: natural vibration and seismic response

5.1. Natural vibration analysis

In this section, the influence of joint stiffness on the natural vibration of the suspend-dome was investigated. In this part, only the weight of the components was considered. Fig. 17 shows the changing tendency of the fundamental frequency to the stiffness factor of the different parts. "ALL" indicates that the joint stiffness of all the parts of the structure was adjusted all together. Thus, the natural frequency will not be influenced when the joint stiffness of each part changed from 0.6 to 1. The natural frequency starts to change when $\alpha 11$ decreased to 0.5, indicating that the vibration modes changed from overall vibration to local vibration, which can be observed in Fig. 18(e) and (f).

Fig. 18 shows the first vibration modes under different conditions. Fig. 18(a) and (b) show the vibration modes when all the component

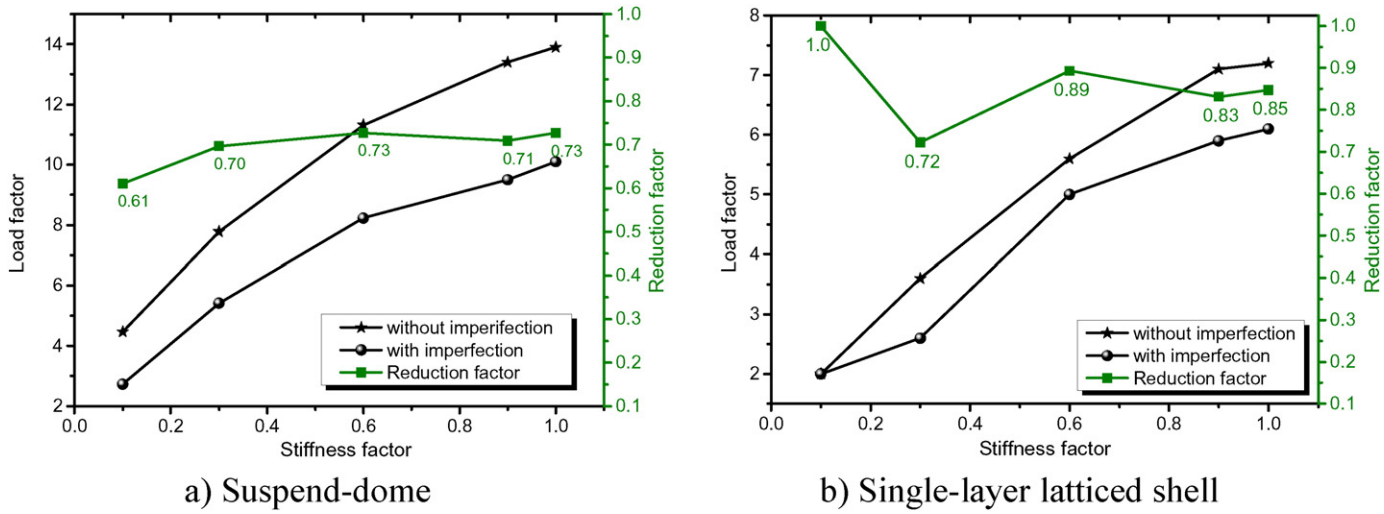

Fig. 16. Changing tendency of load factor along with stiffness factor.

stiffness factors were set to 0.3 and 0.8. When stiffness factors were set to 0.3, the first vibration mode appears to be a local vibration. When the joint stiffness factor increased to 0.8, the vibration mode changes from local vibration to overall vibration.

Fig. 18(c) and (d) show the vibration modes when $\alpha 18$ and $\alpha 17$ were set to 0.1. Thus, vibration occurs at a weak location.

For parameter $\alpha 11$, the fundamental frequency of the overall structure starts to change when it was decreased to 0.5. Fig. 18(e) and (f) show the buckling mode when $\alpha 11$ was set to 0.5 and 0.6. Thus, local vibration occurred when $\alpha 11$ was set to 0.5 and overall vibration happened when it was set to 0.6.

In summary, if joint stiffness factor α ranges from 0.8 to 1, then the error caused by the natural frequency and mode shape can be generally disregarded for the suspend-dome analyzed in this study. The mode shape and natural frequency will deviate from the actual condition when joint stiffness factor α is less than 0.8 if the rigidly connected finite element model was adopted as a substitute for semirigid connected structures. Considering the influence of joint stiffness in calculating the characteristics of natural vibration is necessary.

5.2. Seismic response analysis

The Imperial Valley seismic wave was adopted to conduct seismic response analysis. The time history of the seismic wave is shown in Fig. 19. The peak acceleration in the *x*-direction was adjusted to 55 cm/s^2, and the ratio of the peak value in the *x*-, *y*-, and *z*-directions is 1.00:0.85:0.65. The duration of the seismic wave is 14.7 s. The analysis was conducted in a time step of 0.1 s.

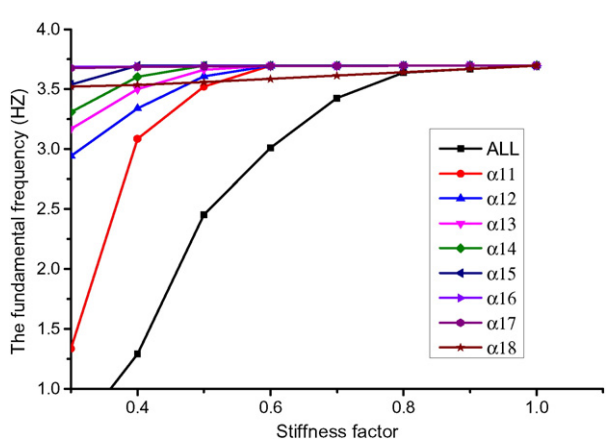

Fig. 17. Curves of fundamental frequency to stiffness factor.

Fig. 20 shows the time history of the displacement at node 1 when stiffness factor α was given a different value. The largest seismic response appears when α was set to 0.6 and approximately twice that when α was set to 1.0. The minimum seismic response occurs when α was set to 0.1. When α was set to 0.1, the natural frequency of the overall structure is relatively small for the deviation to occur from the main frequency component of the selected seismic wave, which is the cause of minimum seismic response. The response reaches the maximum value in the front part of the seismic wave, which varies from the others.

The joint stiffness generally adopted in actual structures is between 1 and 0.5. Thus, the analysis was added to obtain more detailed results. The time history of the vertical displacement at node 1 is shown in Fig. 21(a). The peak value of each case was extracted, as presented in Fig. 21(b). Thus, joint stiffness significantly affects the seismic response of suspend-dome structures. The seismic response of semirigidly connected structures is larger than that of rigidly connected structures by approximately 1.4 times. Substituting rigidly connected models for semirigid models is unsafe. Almost all actual projects are semirigidly connected. Joint stiffness should be considered in calculating the seismic response during the design phase.

5.3. Influence of boundary condition

The influence of boundary condition on structural dynamic response was investigated. The stiffness of the bearing located at the fourth outmost ring, as shown in Fig. 8(b), was adjusted to investigate the influence of boundary condition. The value of bearing stiffness in the hoop direction differed, and the results in each case were derived.

The effect of bearing stiffness on structural dynamic response is shown in Fig. 22. The results indicate that the structural dynamic response was significantly influenced by bearing stiffness when the stiffness factor ranged from 0.4 to 0.7. Regardless of the value of the bearing stiffness, the maximum vertical displacement reaches the minimum value when stiffness was set to 0.3 and 0.9. In addition, the dynamic response of the semirigidly connected structure is significantly higher than the pinned or rigid connected structures regardless of the value of the bearing stiffness.

6. Conclusions

The double element method was adopted in this study to conduct a detailed analysis of suspend-dome structures. First, the accuracy of this method was validated. The model was adopted to analyze the influence

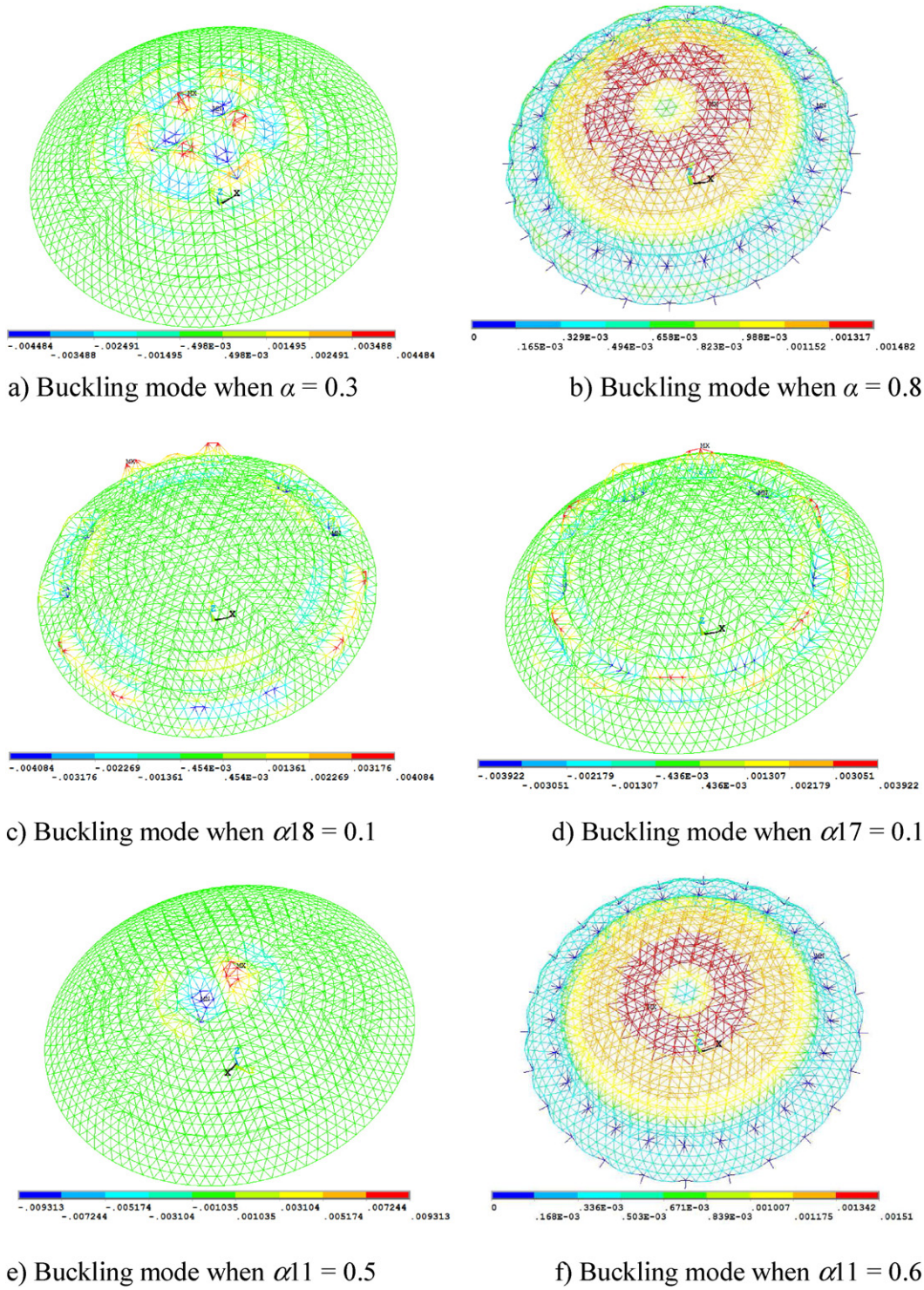

Fig. 18. Buckling mode with different stiffness factors.

of joint stiffness on the mechanical behavior of the overall structure. Buckling, modal, and dynamic response analyses were conducted. The conclusions can be summarized as follows:

(1) The double element method proposed in this study can be efficiently conducted in a general finite element software for the mechanical analysis of complex latticed shells. The difficulty of establishing numerical models is avoided.
(2) Joint stiffness of components located in different locations in the overall structure variably affect the buckling capacity of suspend-dome structures. The influence of the upper components is larger than that of the lower components. The influence of hoop components is less than that of the other components.
(3) Geometrical imperfection will reduce structural buckling capacity. However, joint stiffness has almost no influence on this reduction. Thus, the rigidly connected structural models can be employed to estimate the influence of geometrical imperfection. However, this approach will overestimate structural buckling capacity.
(4) The error caused by natural frequency and mode shape can be neglected if joint stiffness factor α ranges from 0.8 to 1 for the

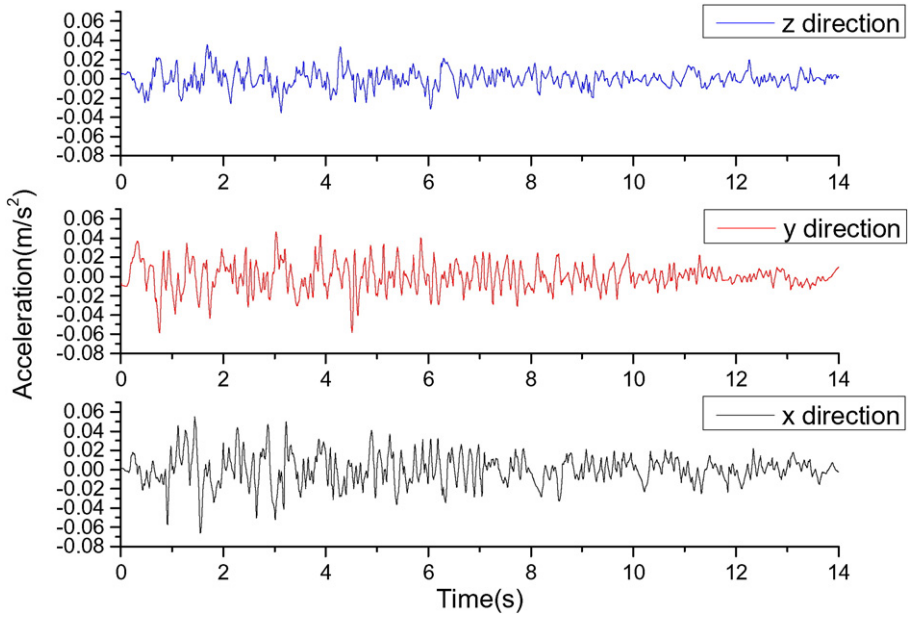

Fig. 19. Time history of the Imperial Valley seismic wave.

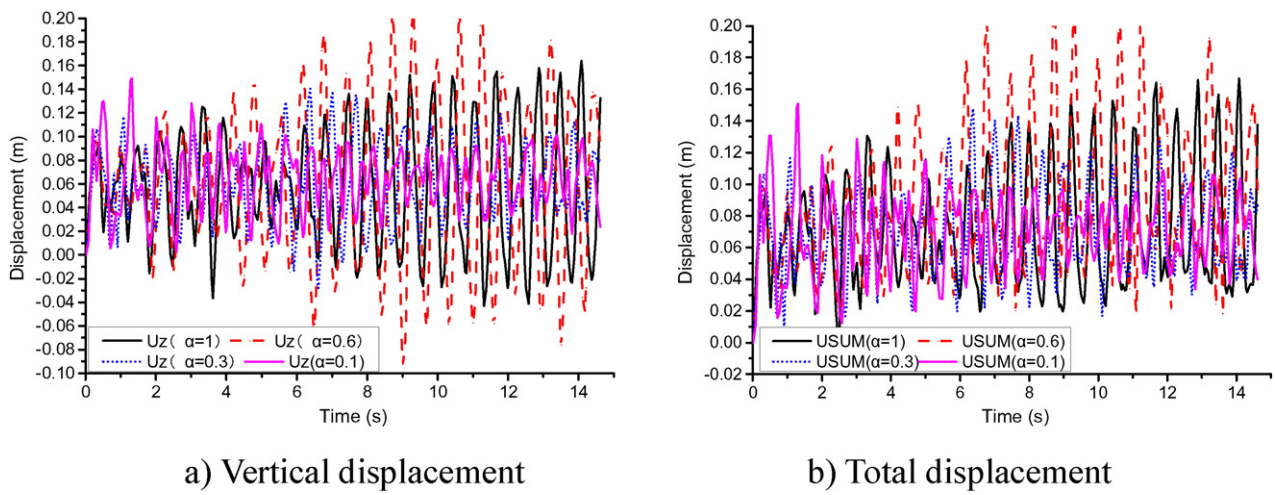

Fig. 20. Time history of displacement at node 1.

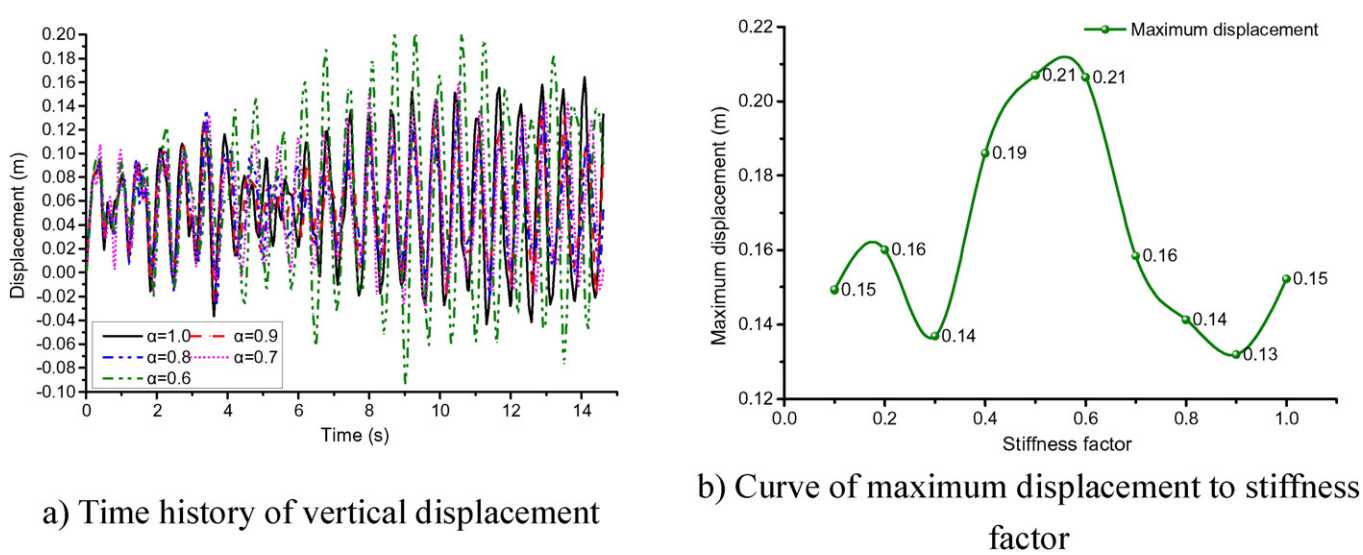

Fig. 21. Comparison of maximum displacement.

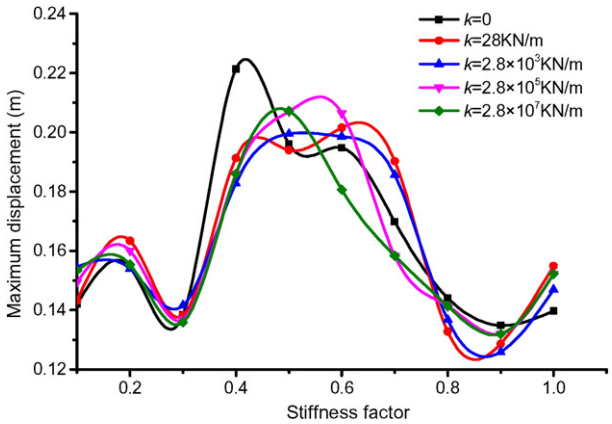

Fig. 22. Influence of bearing stiffness on dynamic response.

suspend-dome analyzed in this study. Mode shape and natural frequency will deviate from the actual condition when joint stiffness factor α is less than 0.8 if the rigidly connected finite element model was adopted as a substitute for semirigid connected structures. Considering the influence of joint stiffness in calculating the characteristics of natural vibration is necessary.

(5) Dynamic response analysis of semirigid structures may yield larger results than that by rigidly connected finite element models. Substituting rigidly connected models for semirigid models is unsafe. Almost all actual projects are semirigidly connected. The joint stiffness should be considered in calculating seismic response during the design phase.

(6) Although the element number of the numerical model established by the double element method was larger than the traditional model, the computational cost was acceptable. Five seconds are required to conduct linear buckling analysis at one time, 170 s to conduct nonlinear buckling analysis at one time, and 15 min to conduct seismic response analysis at one time.

7. Future work

A novel numerical method considering joint stiffness was proposed in this study. The influence of joint stiffness on structural mechanical behavior can be systematically investigated using this method. In addition to joint stiffness, other factors, such as component axial stiffness and residual stress, will also influence buckling behavior. These factors may be investigated in future work.

Acknowledgments

The work described in this paper was fully supported by the National Science Foundation of China (No. 51408414).

References

[1] Zhen Zhou, Jing Wu, Shaoping Meng, Influence of member geometric imperfection on geometrically nonlinear buckling and seismic performance of suspen-dome structures, Int. J. Struct. Stab. Dyn. 14 (3) (2014) 1–20.
[2] Chen ZhiHua, Qin YaLi, Zhao JianBo, Yun Guo, Du KaiLiang, Li Yang, An experimental study on rigid suspendome structures, China Civ. Eng. J. 39 (9) (2006) 47–53 (in Chinese).
[3] Chen ZhiHua, Suspen-Dome Structures, Science Press, Beijing, China, 2010 (in Chinese).
[4] Chen ZhiHua, Liu HongBo, XiaoDun Wang, Zhou Ting, Establishing and application of cable-sliding criterion equation, Adv. Steel Constr. 7 (2) (2011) 131–143.
[5] JiaMin Guo, ShiLin Dong, Yuan XingFei, Morphological analysis of suspendome structures and practical analysis method, China Civ. Eng. J. 41 (2) (2008) 1–7 (in Chinese).
[6] Kang Wenjiang, Chen Zhihua, Lam HeungFai, Zuo Chenran, Analysis and design of the general and outmost-ring stiffened suspen-dome structures, Eng. Struct. 25 (3) (2003) 1685–1695.
[7] S. Kitipornchai, Wenjiang Kang, Heung-Fai Lam, F. Albermani, Factors affecting the design and construction of Lamella suspen-dome systems, J. Constr. Steel Res. 61 (6) (2005) 764–785.
[8] Huihuan Ma, Feng Fan, Gengbo Chen, Zhenggang Cao, Shizhao Shen, Numerical analyses of semi-rigid joints subjected to bending with and without axial force, J. Constr. Steel Res. 90 (2013) 13–28.
[9] Wang Yuanqing, Cao Yulong, Ding Dayi, Zhu Weiliang, Wang Lei, Finite element analysis of key joint test capacity of national financial information building, J. Tianjin Univ. 47 (S) (2014) 118–123 (in Chinese).
[10] A.M. Altuna Zugasti, A. Lopez-Arancibia, I. Puente, Influence of geometrical and structural parameters on the behaviour of squared plan-form single-layer structures, J. Constr. Steel Res. 72 (2012) 219–226.
[11] Aitziber López, Iñigo Puente, Miguel A. Serna, Direct evaluation of the buckling loads of semi-rigidly jointed single-layer latticed domes under symmetric loading, Eng. Struct. 29 (1) (2007) 101–109.
[12] Aitziber López, Iñigo Puente, Miguel A. Serna, Numerical model and experimental tests on single-layer latticed domes with semi-rigid joints, Comput. Struct. 85 (7) (2007) 360–374.
[13] A. Loureiro, R. Goni, E. Bayo, A one-step method for buckling analysis of single layer latticed structures with semi-rigid connections, Proceedings of the fifth International Conference of Space Structures, Thomas Telford, London 2002, pp. 1481–1490.
[14] Huihuan Ma, Feng Fan, Shizhao Shen, Numerical parametric investigation of single-layer latticed domes with semi-rigid joints, J. Int. Assoc. Shell Spat. Struct. 49 (2) (2008) 99–110.
[15] Shiro Kato, Itaru Mutoh, Masaaki Shomura, Collapse of semi-rigidly jointed reticulated domes with initial geometric imperfections, J. Constr. Steel Res. 48 (2–3) (1998) 145–168.
[16] Fan Feng, Huihuan Ma, Cao Zhenggang, Shizhao Shen, A new classification system for the joints used in lattice shells, Thin-Walled Struct. 49 (12) (2011) 1544–1553.
[17] Huihuan Ma, Feng Fan, Jie Zhong, Zhenggang Cao, Stability analysis of single-layer elliptical paraboloid latticed shells with semi-rigid joints, Thin-Walled Struct. 72 (2013) 128–138.
[18] Huihuan Ma, Feng Fan, Peng Wen, Hao Zhang, Shizhao Shen, Experimental and numerical studies on a single-layer cylindrical reticulated shell with semi-rigid joints, Thin-Walled Struct. 86 (2015) 1–9.
[19] J.J. del Coz Díaz, P.J. García Nieto, M. Fernández Rico, J.L. Suárez Sierra, Non-linear analysis of the tubular 'heart' joint by FEM and experimental validation, J. Constr. Steel Res. 63 (8) (2007) 1077–1090.
[20] Minas E. Lemonis, Charis J. Gantes, Mechanical modeling of the nonlinear response of beam-to-column joints, J. Constr. Steel Res. 65 (4) (2009) 879–890.
[21] Mohammad Razavi, Ali Abolmaali, Earthquake resistance frames with combination of rigid and semi-rigid connections, J. Constr. Steel Res. 98 (2014) 1–11.
[22] J.G.S. da Silva, L.R.O. de Lima, P.C.G. da S. Vellasco, P.C.G. de Andrade, P.C.G. da S. Vellasco, R.A. de Castro, Nonlinear dynamic analysis of steel portal frames with semi-rigid connections, Eng. Struct. 30 (9) (2008) 2566–2579.
[23] Li Bai, M. Ahmer Wadee, Mode interaction in thin-walled I-section struts with semi-rigid flange–web joints, Int. J. Non-Linear Mech. 69 (2015) 71–83.
[24] Beatriz Gil, Rufino Goñi, Eduardo Bayo, Experimental and numerical validation of a new design for three-dimensional semi-rigid composite joints, Eng. Struct. 48 (2013) 55–69.
[25] Fernando Busato Ramires, Sebastião Arthur Lopes de Andrade, Pedro Colmar Gonçalves da Silva Vellasco, Luciano Rodrigues Ornelas de Lima, Genetic algorithm optimization of composite and steel endplate semi-rigid joints, Eng. Struct. 45 (2012) 177–191.
[26] ANSYS, Multiphysics 10.0. Canonsburg, Ansys Inc, Pennsylvania, 2003.
[27] M.A. Crisfield, A fast incremental/iterative solution procedure that handles snap-through, Comput. Struct. 13 (1–3) (1981) 55–62.
[28] M.A. Crisfield, An arc-length method including line searches and accelerations, Int. J. Numer. Methods Eng. 19 (1983) 1269–1289.
[29] JGJ61-2003, Technical Specification for Latticed Shells, China Architecture & Building Press, Beijing, China, 2003 (in Chinese).